

LUDWIGS-MAXIMILIANS-UNIVERSITÄT MÜNCHEN  
— DEPARTMENT FOR PHYSICS —

UNIVERSITY OBSERVATORY

# Computational Methods in Astrophysics

## *N*-body Simulations and Galaxy Formation

Version 0.42

Klaus Dolag and Tادziu Hoffmann  
(updated from an earlier version by Thorsten Naab)

30. 10. 2024

---

# Contents

<b>1. Introduction</b>	<b>1-1</b>
1.1. Numerical simulations of interacting galaxies . . . . .	1-5
<b>2. Theoretical background</b>	<b>2-1</b>
2.1. Numerical methods . . . . .	2-1
2.1.1. The Tree Structure – Organizing Particles for Quick Access . . . . .	2-1
2.2. Relaxation and stability of $N$ -body simulations . . . . .	2-2
2.2.1. Time integration . . . . .	2-3
2.3. The initial conditions . . . . .	2-5
2.3.1. Dynamics of collisionless stellar systems . . . . .	2-5
2.3.2. A model for individual galaxies . . . . .	2-7
<b>3. Exercise</b>	<b>3-1</b>
3.1. Fortran vs. Python lab . . . . .	3-1
3.2. Getting used to the data . . . . .	3-2
3.2.1. Setup . . . . .	3-2
3.2.2. Visualizing the initial conditions . . . . .	3-2
3.3. Preparing vine_3D . . . . .	3-2
3.4. Dynamical evolution of a single disk in isolation . . . . .	3-3
3.5. A galaxy merger simulation . . . . .	3-6
3.6. Further interpretation and exploration . . . . .	3-7



# Chapter 1

## Introduction

It is the goal of this exercise that you are introduced to  $N$ -body simulations, a modern technique used in computational astrophysics to investigate the formation and evolution of galaxies, the basic building blocks of our universe. You learn how particle models for disk galaxies are set up and how their dynamical evolution can be simulated using numerical methods. In the astrophysical context this is particularly important for understanding galaxy interactions which are observed in the far and nearby universe.

Toomre & Toomre (1972) invented the idea that dynamically hot elliptical galaxies could originate from mergers of dynamically cold disk galaxies. This “merger hypothesis” has become one of the most popular formation scenarios for elliptical galaxies. Therefore the study of nearby interacting systems – if they evolve into elliptical galaxies at all – will help to illuminate the important mechanisms responsible for the observed properties of elliptical galaxies in general. In the local universe there are several candidates for merging gas-rich disk galaxies. The “Antennae” galaxies (NGC 4038/39) are the classic example of a nearby system composed of two overlapping late-type spiral galaxies in an early phase of a merger. The long extended tails most likely have a tidal origin and are characteristic for gravitationally interacting spiral galaxies. The merger of the Antennae galaxies is accompanied by several bursts of star formation in the two nuclei and the surrounding spiral arms. The most intense burst, however, takes place in an off-nucleus region where the two galaxy disks overlap (Figure 1.1; Mirabel et al., 1998). Here the most massive star clusters form. They are not visible at optical wavelengths since this region is heavily obscured by dust. Most of the energy from this region is emitted by dust which is heated by an intense starburst within giant molecular clouds. This emission can only be measured at infrared wavelengths. In addition, exploding supernovae in starburst regions heat the surrounding gas very effectively. These hot gas bubbles are emitting at X-ray wavelengths (see Figure 1.1).

The Antennae galaxies, at a distance of 20 Mpc, have a total infrared luminosity of  $L_{\text{ir}} \approx 10^{11} L_{\odot}$ , which is about five times its luminosity at optical wavelengths. Therefore the Antennae galaxies belong to the class of luminous infrared galaxies (LIRGs). At luminosities  $L_{\text{bol}} \geq 10^{11} L_{\odot}$ , LIRGs become the dominant population of galaxies in the local universe (see Sanders & Mirabel, 1996). They emit more energy in the infrared ( $5 \dots 500 \mu\text{m}$ ) than at all other wavelengths combined. At luminosities of  $L_{\text{ir}} \geq 10^{12} L_{\odot}$  (ultra luminous infrared galaxies = ULIRGs) all sources are very gas- and dust-rich interacting systems. A small percentage ( $\approx 7\%$ ) of ULIRGs can be considered to be fully relaxed systems with no signs of interaction,  $\approx 22\%$  already completed the merger process and show no second nucleus, and  $\approx 50\%$  of ULIRGs are still interacting, since both nuclei can be identified on the images (Rigopoulou et al., 1999). Clearly, the ULIRGs in the local neighborhood can not explain the formation of elliptical galaxies with

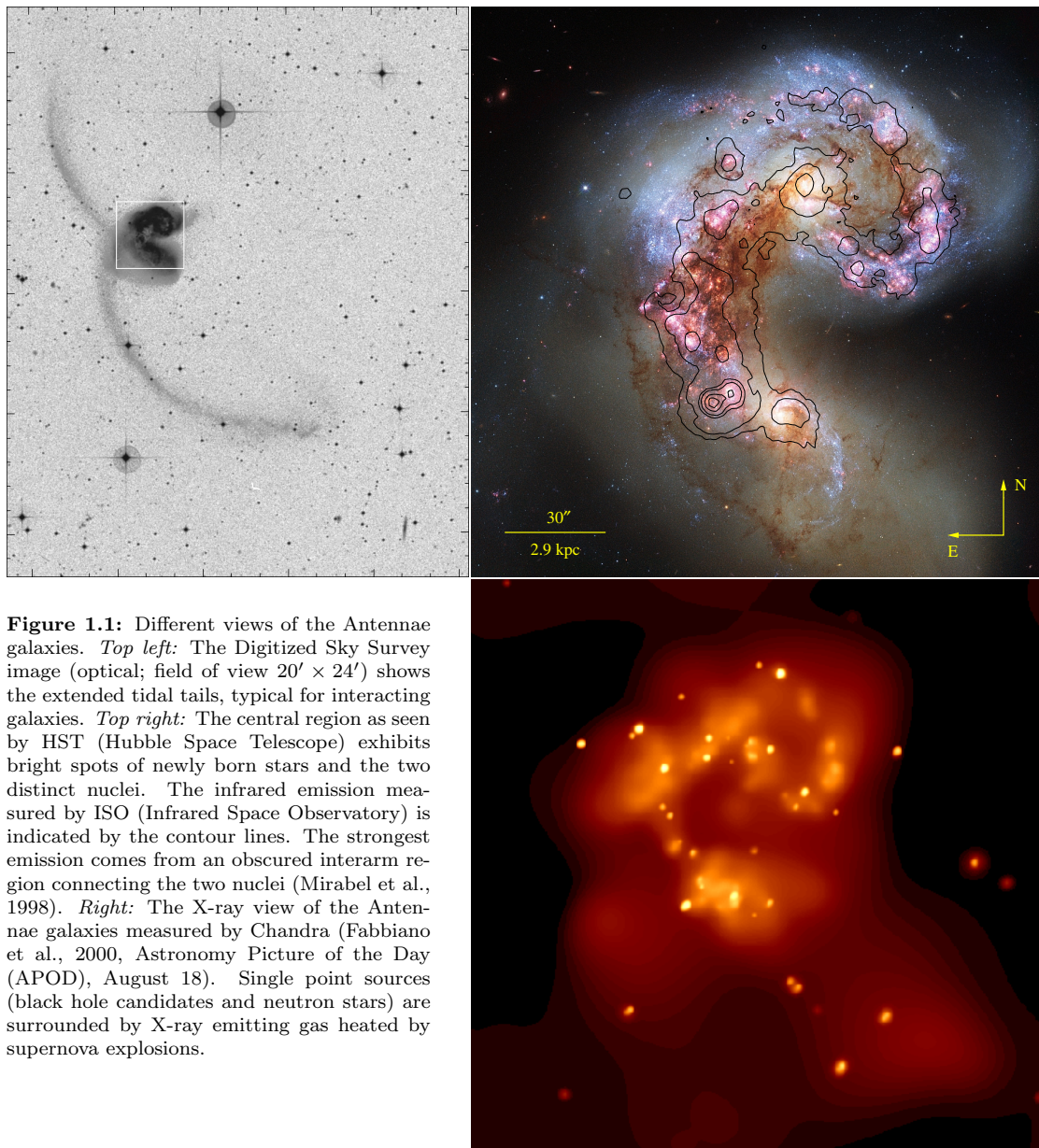


**Figure 1.1:** Different views of the Antennae galaxies. *Top left:* The Digitized Sky Survey image (optical; field of view  $20' \times 24'$ ) shows the extended tidal tails, typical for interacting galaxies. *Top right:* The central region as seen by HST (Hubble Space Telescope) exhibits bright spots of newly born stars and the two distinct nuclei. The infrared emission measured by ISO (Infrared Space Observatory) is indicated by the contour lines. The strongest emission comes from an obscured interarm region connecting the two nuclei (Mirabel et al., 1998). *Right:* The X-ray view of the Antennae galaxies measured by Chandra (Fabbiano et al., 2000, Astronomy Picture of the Day (APOD), August 18). Single point sources (black hole candidates and neutron stars) are surrounded by X-ray emitting gas heated by supernova explosions.

an age of 5 to 10 Gyrs or more. However, Hibbard & Vacca (1997) have shown that ULIRGs are the best local analogues of disturbed high redshift galaxies observed in the Hubble Deep Field (see <http://antwrp.gsfc.nasa.gov/apod/> for further observations) or other deep fields with respect to their morphology, star formation rate, and spectral energy distribution. ULIRGs are therefore good candidates to represent a primary state in the formation of elliptical galaxy cores.

The question whether gas-rich mergers evolve into systems that resemble present day elliptical galaxies is still not fully explored. The “Toomre Sequence” (Toomre, 1977; see also Toomre & Toomre, 1972) of the 11 foremost examples of ongoing mergers of late-type spiral galaxies selected from the New General Catalogue (NGC) provides considerable insight into the merger

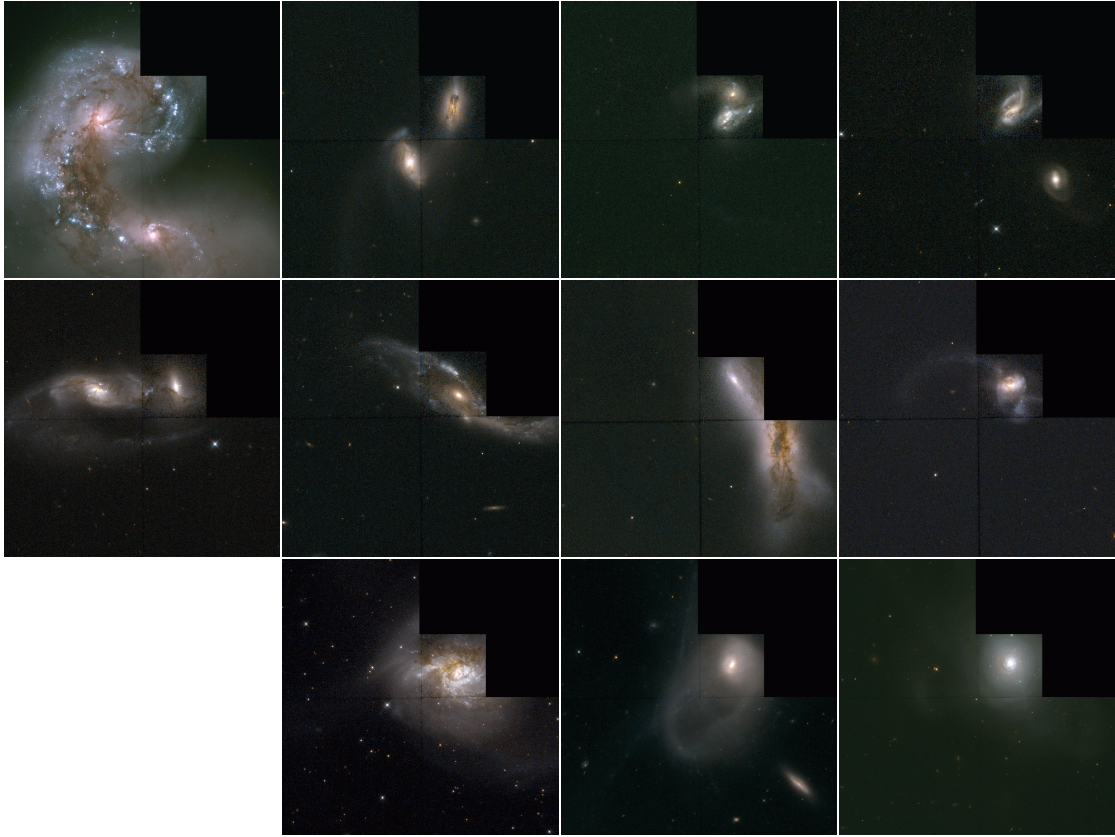


**Figure 1.2:** The Toomre sequence of merging galaxies seen at different phases, observed with HST. From well-separated systems on the upper left to merged systems on the lower right you see: NGC 4038/9, NGC 4676, NGC 7592, NGC 7764A, NGC 6621/2, NGC 3509, NGC 520, NGC 2623, NGC 3256, NGC 3921, and NGC 7252. (Source: <http://www.cv.nrao.edu/~jhibbard/TSeqHST/>.)

process (see Figure 1.2). The optically selected sequence represents the proposed stages of merging disk galaxies. Early-stage mergers have well-separated but distorted disk components (Antennae, Arp 295, NGC 4676, and others). Intermediate-stage mergers exhibit distinct nuclei in a common envelope of luminous material with clear signs of interaction as extended tidal tails (e.g., NGC 520). Late-stage mergers consist of a dynamically relaxed central part with tidal appendages emanating from a single nucleus (e.g., NGC 3921, NGC 7252, Arp 220; Figure 1.3; see Hibbard & van Gorkom, 1996).

A recent study of 3 late-stage mergers has shown that the luminosity profile in the case of NGC 3921 and NGC 7252 (see Figure 1.3) will evolve to an  $r^{1/4}$  law, which is typical for elliptical galaxies. However, Arp 220 (Figure 1.3), which is the most luminous galaxy in the local universe and belongs to the class of ULIRGs, shows an excess of light in the central part. This excess of light is not a common feature among elliptical galaxies. It is found only in some cores of ellipticals. However, different processes like powerful expanding super-winds or massive starbursts with an initial mass function that is biased towards massive stars can lead to reduced central stellar densities when Arp 220 evolves with time. Observed physical processes taking place in interacting galaxies in the local universe are dominated by gas dynamics and star formation. The role of stellar dynamics, however, is difficult to estimate.

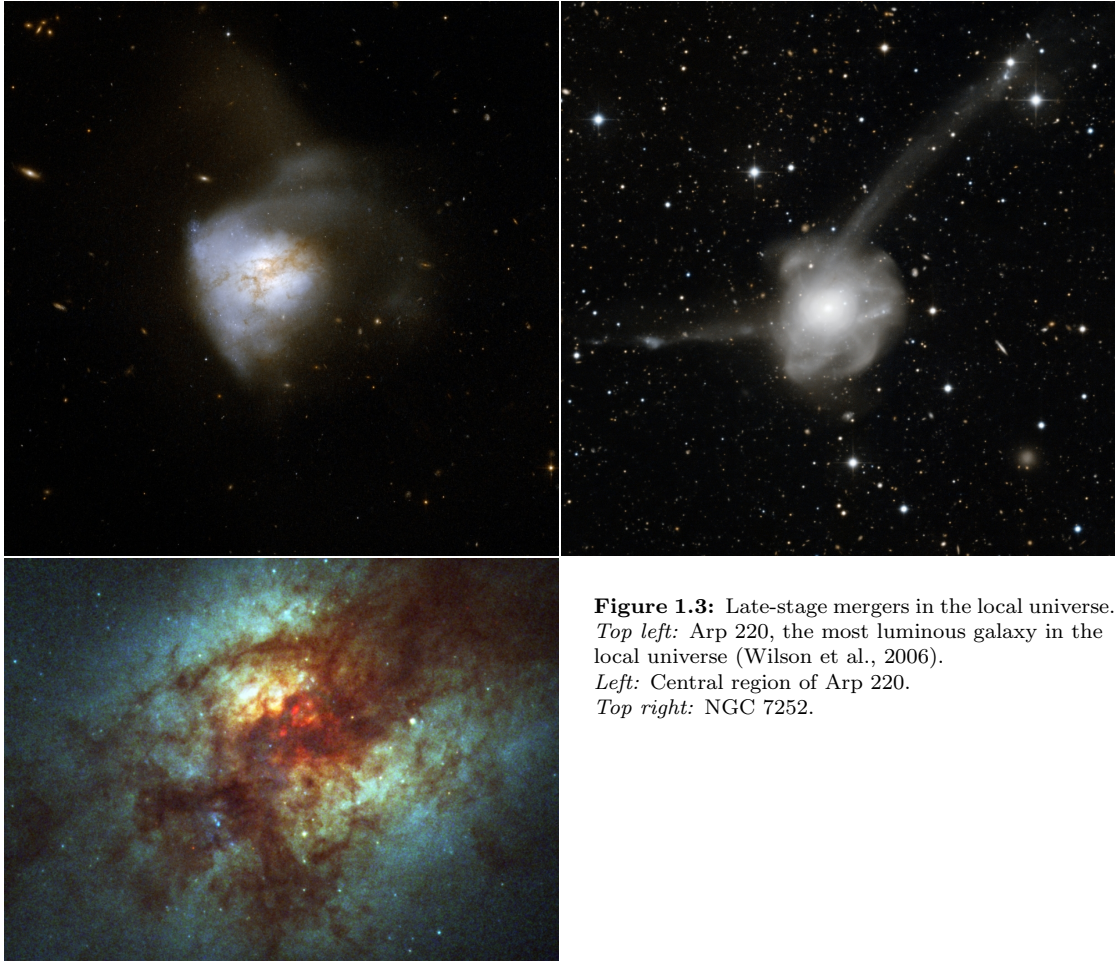


**Figure 1.3:** Late-stage mergers in the local universe.  
*Top left:* Arp 220, the most luminous galaxy in the local universe (Wilson et al., 2006).  
*Left:* Central region of Arp 220.  
*Top right:* NGC 7252.

Dynamical modeling has demonstrated that large scale interactions are efficient means of driving central inflows of gas and therefore can trigger nuclear starbursts or AGNs as energy sources for the enormous infrared emission seen in ULIRGs (see e.g., Barnes & Hernquist, 1996). However, the detailed processes leading to a starburst are not well understood. Up to now, numerical simulations which include stellar dynamics, gas dynamics, star formation and its feedback were not able to reproduce all the observed features (Mihos & Hernquist, 1996; Barnes & Hernquist, 1996; see Hibbard & Yun, 1999). In particular, there are several questions that have to be addressed in detail. How much gas in total is needed to get the high densities observed in centers of elliptical galaxies? What is the influence of gas on the global dynamics of merger remnants? When, where, and how does the gas transform into stars? Where does the hot X-ray emitting gas, observed in massive giant elliptical galaxies, come from? Does gas accrete onto a central black hole? How does the existence of a black hole influence the dynamics of the remnant? What is the influence of magnetic fields? However, all these questions involve complicated physical processes that are either poorly understood theoretically – such as star formation in molecular clouds – or involve complicated physics and are very difficult to implement numerically, like magnetic fields or relativistic hydrodynamics.

There exists a lot of detailed information about central and global photometry, global kinematical properties and spatially resolved local kinematics of giant elliptical galaxies. This data can be compared with dynamical models of interacting galaxies. It is remarkable that even collisionless dynamical models which only involve gravitation have only been investigated to a small extent. In particular, it is not clear in how far collisionless mergers succeed or fail to explain the formation of elliptical galaxies by collisionless mergers of disk galaxies.

## 1.1. Numerical simulations of interacting galaxies

In the 1970s, Toomre & Toomre (1972) and later on Toomre (1977) proposed on the basis of experiments with a restricted 3-body method that early type galaxies could originate from mergers of disk galaxies. Almost at the same time Ostriker & Tremaine (1975) suggested that dynamical friction and repeated mergers and accretion of galaxies near the centers of galaxy clusters could be responsible for the formation of massive cD galaxies. This *merger hypothesis* has become one of the most popular models for the formation of elliptical galaxies. The merger hypothesis has been tested in great detail by many authors. White (1978, 1979) investigated mergers of spherical galaxies, Gerhard (1981), Farouki & Shapiro (1982) and, later on, Negroponte & White (1983) were among the first who performed self-consistent merger simulations of disk galaxies. However, the resolution of these simulations was very low and the number of particles representing each galaxy did not exceed 500. The situation changed with the advent of Treecodes in the late 1980s (Appel, 1985; Jernigan, 1985; Barnes, 1986; Hernquist, 1987; Jernigan & Porter, 1989). The method allowed simulations without restrictions to the geometry of the problem and reduced the computational effort to simulate a system with  $N$  particles from  $\mathcal{O}(N^2)$  to  $\mathcal{O}(N \log N)$ . Using this powerful tool, the merger hypothesis has been investigated by numerous authors in great detail (see Barnes & Hernquist (1992) for a review). Using the Treecode, the first fully self-consistent mergers of two equal mass, rotationally supported disk galaxies embedded in dark halos were performed by Barnes (1988) and Hernquist (1992). They found that mergers indeed lead to slowly rotating, pressure supported anisotropic systems. The remnants were triaxial and showed both disky and boxy isodensity contours in projection (Hernquist, 1992). In addition it was found, in contradiction to the common belief, that mergers of equal mass galaxies lead to the formation of loops and shells around the remnants in good agreement with observations of shells around elliptical galaxies (Hernquist & Spiegel, 1992). The surface density of the remnants simulated by Barnes (1988) contained a central bulge component and followed an  $r^{1/4}$  profile up to the central resolution limit, determined by the gravitational softening length. The half-mass radius of the system was slightly larger than the scale length of the initial disk. The pure disk mergers performed by Hernquist (1992) were too diffuse at the center, leading to strong deviations from the observed surface density profile of elliptical galaxies. This result can be explained by limited phase space densities at the centers of observed disk galaxies that are in disagreement with the high phase space densities at the centers of elliptical galaxies and bulges (Carlberg, 1986; Wyse, 1998). Subsequent investigations by Hernquist et al. (1993b) showed that mergers of progenitors with massive bulge components (25%–30% of the disk mass) could resolve this problem leading to core radii and surface brightness profiles that are in excellent agreement with observations. This result is expected since the mergers already start with galaxies that contain elliptical like components and therefore dissipation may not be needed to satisfy phase space constraints.

It has been argued by Kormendy & Bender (1996), Faber et al. (1997) and Rix et al. (1999) that gaseous mergers lead to distinct inner gaseous disks in the merger remnants which subsequently turn into stars, generating disky isophotes and strong rotational support in the outer regions. In contrast, boxy ellipticals would form from purely dissipationless mergers. This idea

has theoretically been addressed in detail by Bekki & Shioya (1997) and Bekki (1998) and recently by Springel (2000). Bekki & Shioya (1997) simulated mergers including gaseous dissipation and star formation. They found that the rapidity of gas consumption affects the isophotal shapes. Secular star formation however leads to final density profiles which deviate significantly from the observed  $r^{1/4}$  profiles in radial regimes where all ellipticals show almost perfect de Vaucouleurs laws (Burkert, 1993). These calculations and models of Mihos & Hernquist (1996) demonstrate that the effect of gas and star formation changes the structure of merger remnants as such a dissipative component would most likely lead to strong deviations from the  $r^{1/4}$  profiles which seems to be a result of dissipationless, violent relaxation processes. Nevertheless the observations of metal-enhanced, decoupled and rapidly spinning disk-like cores (Bender & Surma, 1992; Davies et al., 1993; Bender & Davies, 1996) show that even in boxy ellipticals gas must have been present. Numerical simulations show that these features would result naturally from gas infall during the merger process (Barnes & Hernquist, 1996; Mihos & Hernquist, 1996). The influence of gas on the global structure of elliptical galaxies is not well understood as it is sensitive to uncertain details about the star formation process (Barnes & Hernquist, 1996).

## Chapter 2

# Theoretical background

### 2.1. Numerical methods

In addition to theoretical and experimental physics, computational physics has become a powerful tool for answering astrophysical questions. The increase of computer power and the development of special hardware and software have opened the opportunity to model the evolution of galaxies directly. The data analysis following such a virtual experiment is then carried out in much the same way as an observer would do with data from a real observation. The  $N$ -body simulation technique has become one of the most powerful tools for the study of astronomical systems of gravitationally interacting subunits: the solar system, star clusters, galaxies, clusters of galaxies, and the large-scale structure of the universe.

#### 2.1.1. The Tree Structure – Organizing Particles for Quick Access

The easiest and initially most intuitive way to compute the gravitational accelerations on the particles is the so called direct summation approach. The force exerted on a particle  $i$  is computed as the sum of the forces from all other particles  $j \neq i$  inside the system. This technique gives the correct acceleration for every particle, but has the major drawback that  $\mathcal{O}(N^2)$  operations are required for the calculation. For simulations of collisionless systems, a small error in the accelerations is, however, tolerable without affecting the evolution of the system. It is thus feasible to implement methods which require less than  $\mathcal{O}(N^2)$  operations while at the same time producing slightly less accurate accelerations for the particles.

The most commonly used technique for computing the accelerations is based on ordering the particles into a tree structure. Instead of actually computing every single interaction with a remote set of particles, a single interaction with a node of the tree structure is computed, where the node contains a corresponding set of particles. The number of operations required for the calculation of the accelerations of all particles decreases to  $\mathcal{O}(N \log N)$ .

A variety of algorithms for building and using such tree structures in astrophysical particle simulations have been developed. The two most important are variants of the so called “octree” and “binary tree” structures. In an octree (Barnes 1986), the tree is built in a top-down fashion: The system is placed into a cube encompassing all particles. Then the cube is split into its eight octants, which are then in turn split accordingly. The procedure repeats until on the lowest level either one or no particles are found inside a cube. These cubes form the leaves of the tree. A binary tree (Appel 1985) is usually built in a bottom-up fashion (see, however, Jernigan & Porter 1989 for an alternative approach and for a comparison of octrees and binary trees). VINE, the

simulation code used for this exercise, follows the original idea for a binary tree by combining nearest neighbor particles into nodes of the tree and repeating the procedure until only one node, the root node, is left. This type of tree structure does not make use of an artificial tessellation of space in order to build the tree and has the advantage of naturally following the geometry of the physical system under consideration.

## 2.2. Relaxation and stability of $N$ -body simulations

In the exercise presented here the gravitational force is computed as

$$\mathbf{F}_i = - \sum_{j \neq i} \frac{Gm_i m_j (\mathbf{x}_i - \mathbf{x}_j)}{(|\mathbf{x}_i - \mathbf{x}_j|^2 + \varepsilon^2)^{3/2}} \quad (2.1)$$

where  $\mathbf{x}_i$  and  $\mathbf{x}_j$  are the positions of particle  $i$  and  $j$  and the softening-parameter  $\varepsilon$  avoids divergence at  $\mathbf{x}_i = \mathbf{x}_j$ .

Many astrophysical stellar systems can be considered as collisionless systems during their evolution (see Section 2.3.1). Two-body encounters are unimportant as well as local deviations from a smooth global potential. For numerical simulations of galaxies which typically contain  $10^{11}$  particles the number of particles is limited to  $10^5 \dots 10^7$  test particles which have typical masses of  $10^4 \dots 10^6$  solar masses, even for the fastest present-day supercomputers. For systems with small particle numbers two-body interactions its relaxation time is artificially reduced (see Section 2.3.1). For two-dimensional models of disks (e.g., Earn & Sellwood, 1995) we can estimate the relaxation time being the time-scale on which stars of similar mass diffuse in velocity space (White, 1988) as:

$$t_R = \frac{\sigma}{\pi G \Sigma} \quad (2.2)$$

where  $\sigma = \sqrt{\sigma_r \sigma_\phi}$  is the velocity dispersion and  $\Sigma$  is the surface density of the disk.

With a radial dispersion of

$$\sigma_r = Q \frac{3.36 G \Sigma}{\kappa} \quad (2.3)$$

and a tangential dispersion of

$$\sigma_\phi = \sigma_r \frac{\kappa}{2\Omega} \quad (2.4)$$

we get a relaxation time which is comparable to the epicyclic period  $2\pi/\kappa$  and therefore the system can not be considered collisionless.

To perform useful simulations the effects of relaxation have to be reduced. One possibility is to introduce a softened force as in Equation 2.1.

The potential at particle  $i$  can be written as

$$\Phi(\mathbf{x}_i) = - \sum_{j \neq i} \frac{Gm_j}{(|\mathbf{x}_i - \mathbf{x}_j|^2 + \varepsilon^2)^{1/2}}. \quad (2.5)$$

where  $m_j$  is the mass of particle  $j$  and  $\varepsilon$  is softening parameter. This type of force softening is also called Plummer-softening as the particle contributed to the potential as if its mass were distributed like a Plummer density profile

$$\rho(\mathbf{x}_i) = - \sum_j \frac{3m_j}{4\pi} \frac{\varepsilon^2}{(|\mathbf{x}_i - \mathbf{x}_j|^2 + \varepsilon^2)^{5/2}}. \quad (2.6)$$

Formally the softening can be interpreted in the following way: define a smooth density at  $\mathbf{x}$  as

$$\rho(\mathbf{x}) = \int W(\mathbf{x} - \mathbf{x}', \varepsilon) \rho_p(\mathbf{x}') d\mathbf{x}' \quad (2.7)$$

with a density of a particle

$$\rho_p(\mathbf{x}) = \sum_j m_j \delta(\mathbf{x} - \mathbf{x}_j) \quad (2.8)$$

and a smoothing-kernel for Plummer-softening

$$W(\mathbf{x} - \mathbf{x}', \varepsilon) = \frac{3}{4\pi} \frac{\varepsilon^2}{(|\mathbf{x} - \mathbf{x}'|^2 + \varepsilon^2)^{5/2}}. \quad (2.9)$$

To some degree the functional form of this kernel is arbitrary. Other density distribution are also possible as long as  $W(\mathbf{x})$  follows  $W(\mathbf{x}) \rightarrow \delta(\mathbf{x})$  for  $\varepsilon \rightarrow 0$  and  $\rho(\mathbf{x}) \geq 0$  for all  $\mathbf{x}$ .

For two-dimensional systems including softening the relaxation time is increased to to (Rybicki, 1971)

$$t_R \approx \frac{\sigma^3 \varepsilon}{\pi G^2 \Sigma m} \quad (2.10)$$

where  $m$  is the particle mass and  $\varepsilon$  is the smoothing length.

In addition to two-body relaxation there exists another, equally important, source for relaxation. Due to the limited number of particles the noise in the particle distribution leads to small-scale fluctuations in the density and the potential. In real 3-dimensional disks short-range encounters as well as long-range encounters contribute to the relaxation of the system and the previous computations are not valid any more. It is therefore important to investigate the stability of a system using different softening lengths under realistic assumptions.

### 2.2.1. Time integration

In  $N$ -body simulations the particles move according to the Newtonian equations of motion

$$\begin{aligned} \frac{d\mathbf{x}}{dt} &= \mathbf{v}, \\ m \frac{d\mathbf{v}}{dt} &= \mathbf{F}. \end{aligned} \quad (2.11)$$

The functional form of  $\mathbf{F}$  depends on the forces that are necessary for the simulations. For  $N$ -body simulations this reduces to the gravitational forces. To integrate this set of equations numerically it is necessary to replace them by linear algebraic relationships. The continuous functions  $\mathbf{x}$  and  $\mathbf{v}$  are replaced by values at discrete time intervals. The most commonly used discretization for  $N$ -body simulations is the *leapfrog* scheme or Verlet method (see Hockney & Eastwood, 1981). It is the standard way of integrating the equations of motion of interacting particles whose interactions do not explicitly depend on velocity, like stellar dynamics. It has been used by a wide variety of authors investigating different problems (Barnes, 1988; Hernquist & Quinn, 1988, Barnes, 1988; Barnes & Hernquist, 1992; Hernquist et al., 1993a; Barnes & Hernquist, 1996; Velazquez & White, 1999 and many others). In this scheme the discretization of the equations (2.11) is realized by

$$\begin{aligned} \mathbf{x}^{(n+1)} &= \mathbf{x}^{(n)} + \mathbf{v}^{(n+\frac{1}{2})} \Delta t, \\ \mathbf{v}^{(n+\frac{1}{2})} &= \mathbf{v}^{(n-\frac{1}{2})} + \frac{\mathbf{F}(\mathbf{x}^{(n)})}{m} \Delta t. \end{aligned} \quad (2.12)$$

Here  $\Delta t$  is the time step and the superscript  $n$  is the time level  $t = n\Delta t$ . This scheme is consistent in the sense that for  $\Delta t \rightarrow 0$  the discretization (2.12) tends towards the continuous equations (2.11). Another desired consistency property is that the discrete approximations and the continuous equations have the same time symmetry. The Newtonian equations of motion are time-reversible, i.e., if a particle is integrated forwards in time on a trajectory and the time arrow is reversed, the particle will follow the same trajectory backwards returning to its starting point. Time reversible discretization are obtained by time-centered difference approximations. In the equations (2.12) the difference  $(\mathbf{x}^{(n+1)} - \mathbf{x}^{(n)})$  is centered about  $t^{(n+\frac{1}{2})}$  and the difference  $(\mathbf{v}^{(n+\frac{1}{2})} - \mathbf{v}^{(n-\frac{1}{2})})$  is centered on  $t^{(n)}$ . The accuracy of the discretization scheme is given by round-off errors in the computer and truncation errors caused by representing the continuous variables by a discrete set of values. For stable integration schemes, round-off errors are smaller than truncation errors and can be neglected. Truncation errors can be seen as the difference between the differential equations and their algebraic approximations. The measure of the smallness of truncation errors is then given by the order  $p$  of the difference scheme, where the error is  $\propto (\Delta t)^p$  for small  $\Delta t$ . If the overall time step  $\Delta t$  is held constant the leapfrog approximation is time-reversible and is a second-order accurate approximation to the equations of motion (see Hockney & Eastwood, 1981).

Replacing  $\mathbf{v}$  in equations (2.12) gives

$$\frac{\mathbf{x}^{(n+1)} - 2\mathbf{x}^{(n)} + \mathbf{x}^{(n-1)}}{(\Delta t)^2} = \frac{\mathbf{F}(\mathbf{x}^{(n)})}{m}. \quad (2.13)$$

If  $\mathbf{X}$  is a solution to the differential equations (2.11),

$$\frac{d^2 \mathbf{X}}{dt^2} = \frac{\mathbf{F}}{m}, \quad (2.14)$$

then we define the error at every time step  $n$  as  $\delta^n$  using equation (2.13)

$$\frac{\mathbf{X}^{(n+1)} - 2\mathbf{X}^{(n)} + \mathbf{X}^{(n-1)}}{(\Delta t)^2} = \frac{\mathbf{F}(\mathbf{X}^{(n)})}{m} - \delta^n. \quad (2.15)$$

After expanding  $\mathbf{X}^{(n+1)}$  and  $\mathbf{X}^{(n-1)}$  in a Taylor series around  $\mathbf{X}^{(n)} = \mathbf{X}(t^{(n)})$  this can be written as

$$\frac{d^2 \mathbf{X}}{dt^2} + \frac{(\Delta t)^2}{12} \frac{d^4 \mathbf{X}}{dt^4} + \text{higher order terms} = \frac{\mathbf{F}(\mathbf{X}^{(n)})}{m} - \delta^n. \quad (2.16)$$

Combining with equation (2.14) we get

$$\delta^n = -\frac{(\Delta t)^2}{12} \frac{d^4 \mathbf{X}}{dt^4} + \text{higher order terms}. \quad (2.17)$$

In addition, the leapfrog scheme is stable for a small enough time step  $\Delta t$ . How the time step has to be adjusted depends on the system that has to be integrated. For hydrodynamical simulations a criterion could be phrased as no information is allowed to travel farther than one resolution unit within one time step. For dynamical simulations the time step must be small enough to resolve the dynamics of the system. A typical value for a time step of a collisionless system is  $10^{-2} \dots 10^{-3}$  dynamical time scales. Small errors at any stage of the integration then do not lead to larger cumulative errors. In addition, the leapfrog scheme is easy to implement and requires little memory. If the time step is properly adjusted to the parameters of the simulations the scheme provides a good compromise between accuracy, stability and efficiency (Athanasoula, 1993; Barnes, 1998).

## 2.3. The initial conditions

Determining initial conditions for numerical simulations of disk galaxies is problematic in general. Galaxies are compound objects consisting of a luminous disk with interstellar gas, a stellar bulge or a bar, and an extended dark halo. The overall goal is to describe a dynamical equilibrium model with physical properties according to observations of the Milky Way and other galaxies. Unfortunately, the distribution function that describes the dynamical evolution of a collisionless system like a galaxy (see Section 2.3.1) is very complex and not well known for systems of such a complexity. One way out is to realize only part of the galaxy with particles and describe the other components by fixed analytic potentials. The disadvantage of those methods is that they do not allow self-consistent interaction between the subsystems. In the standard cosmological model where dark matter halos consist of self-gravitating and collisionless particles those interactions are of fundamental importance for the evolution of the system as a whole.

### 2.3.1. Dynamics of collisionless stellar systems

The dynamics of collisionless stellar systems is discussed extensively in the literature (e.g., Binney & Tremaine, 1987). Therefore we will focus only on the basic concepts that are needed to understand the description of the model for initial conditions in Section 2.3.2.

Gravitationally interacting stars in a galaxy can be assumed to form a collisionless dynamic system. Collisionless means that the motion of a star in a galaxy is determined by the overall potential of the system rather than by interactions with stars close by. Whether a stellar system can be assumed to be collisionless is determined by its relaxation time  $t_{\text{relax}}$ . The relaxation time gives the time-scale after which a star that moves in a system of  $N$  stars is deflected significantly by close encounters with nearby particles from its mean trajectory. The relaxation time can be defined as (see Binney & Tremaine (1987) for details)

$$t_{\text{relax}} = \frac{r_g}{v_t} \frac{N}{8 \ln N}. \quad (2.18)$$

Here  $r_g/v_t = t_{\text{cross}}$  is the crossing time for a system of  $N$  particles with masses  $m$ , and the characteristic radius  $r_g$  is defined as

$$r_g \equiv \frac{GM^2}{|W|}. \quad (2.19)$$

$G$  is the gravitational constant,  $W$  is the total potential energy of the system, and  $M = Nm$  is its total mass.  $v_t$  is the typical velocity

$$v_t^2 \approx \frac{GNm}{R} \quad (2.20)$$

of a particle in such a system with radius  $R$ . Galaxies consisting of  $N = 10^{11}$  particles have relaxation times comparable to the age of the universe and can therefore be assumed to be collisionless systems. It has to be noted that every stellar system can be treated as a collisionless system if it is investigated on timescales significantly smaller than its relaxation time.

In classical mechanics the state of a system of particles is determined by the position  $\mathbf{x}$  and velocity  $\mathbf{v}$  of every particle. Using a discrete set of Newtonian equations of motion it is then possible to determine the velocities and positions of every particle at every time. For the large number of particles involved in stellar dynamical processes it is not possible to follow exactly the trajectory of every particle. Since the particles in a collisionless system move under the influence of a smooth global potential  $\Phi(\mathbf{x}, t)$ , a continuous description of the system is more useful. The state of the system can be given by the number of stars  $f(\mathbf{x}, \mathbf{v}, t) d^3\mathbf{x} d^3\mathbf{v}$  in a volume  $d^3\mathbf{x}$

centered on  $\mathbf{x}$  and velocities in the range  $d^3\mathbf{v}$  centered on  $\mathbf{v}$ . The function  $f(\mathbf{x}, \mathbf{v}, t) \geq 0$ , defined in the 6-dimensional phase-space  $(\mathbf{x}, \mathbf{v})$ , is called the phase-space density or the distribution function of the system. To find a dynamical equation for  $f(\mathbf{x}, \mathbf{v}, t)$ , it can be assumed that the flow of matter through phase space can be described by a 6-dimensional vector  $(\dot{\mathbf{x}}, \dot{\mathbf{v}})$  with

$$(\dot{\mathbf{x}}, \dot{\mathbf{v}}) = (\mathbf{v}, -\nabla\Phi(\mathbf{x}, t)), \quad (2.21)$$

where  $\Phi(\mathbf{x}, t)$  is the gravitational potential. The flux  $(\dot{\mathbf{x}}, \dot{\mathbf{v}})$  is conservative, therefore the change of mass in a phase-space volume  $d\mathbf{x} d\mathbf{v}$  is determined by inflow minus outflow, so

$$\frac{\partial f}{\partial t} + \frac{\partial}{\partial \mathbf{x}} \cdot (f\mathbf{x}) + \frac{\partial}{\partial \mathbf{v}} \cdot (f\mathbf{v}) = 0. \quad (2.22)$$

If we substitute equation (2.21) we obtain the collisionless Boltzmann equation (CBE)

$$\frac{\partial f}{\partial t} + \mathbf{v} \cdot \nabla f - \nabla\Phi \cdot \frac{\partial f}{\partial \mathbf{v}} = 0. \quad (2.23)$$

This equation is the fundamental equation of stellar dynamics. It has the property

$$\frac{df}{dt} = 0. \quad (2.24)$$

*This means that the local phase-space density  $f$  around a phase point of a given star always remains the same* (Binney & Tremaine, 1987). The potential of a given density distribution  $\rho(\mathbf{x})$  is given by the Poisson equation

$$\Delta\Phi(\mathbf{x}, t) = 4\pi G\rho(\mathbf{x}, t) = 4\pi G \int f(\mathbf{x}, \mathbf{v}, t) d^3\mathbf{v}. \quad (2.25)$$

If a distribution function satisfies the Poisson equation (2.25) and the CBE (2.23) it provides a self-consistent solution to a collisionless problem. In the following equations we use the standard summation convention.

One can derive a continuity equation by integrating equation (2.23) over all possible velocities:

$$\int \frac{\partial f}{\partial t} d^3\mathbf{v} + \int v_i \frac{\partial f}{\partial x_i} d^3\mathbf{v} - \frac{\partial\Phi}{\partial x_i} \int \frac{\partial f}{\partial x_i} d^3\mathbf{v} = 0. \quad (2.26)$$

For a spatial density of stars  $\nu(\mathbf{x})$  and a mean stellar velocity  $\bar{\mathbf{v}}(\mathbf{x})$  defined by

$$\nu \equiv \int f d^3\mathbf{v}, \quad \bar{v}_i \equiv \int f v_i d^3\mathbf{v}, \quad (2.27)$$

this simplifies to the continuity equation

$$\frac{\partial \nu}{\partial t} + \frac{\partial(\nu \bar{v}_i)}{\partial x_i} = 0. \quad (2.28)$$

If we multiply the CBE by  $v_j$  and integrate over all velocities we obtain

$$\frac{\partial}{\partial t} \int f v_i d^3\mathbf{v} + \int v_i v_j \frac{\partial f}{\partial x_i} d^3\mathbf{v} - \frac{\partial\Phi}{\partial x_i} \int v_j \frac{\partial f}{\partial v_i} d^3\mathbf{v} = 0. \quad (2.29)$$

Using the fact that  $f \rightarrow 0$  for large  $v$  and applying the divergence theorem, equation (2.29) can be written as

$$\frac{\partial \nu \bar{v}_j}{\partial t} + \frac{\partial(\nu \bar{v}_i \bar{v}_j)}{\partial x_i} + \nu \frac{\partial\Phi}{\partial x_j} = 0, \quad (2.30)$$

with

$$\overline{v_i v_j} \equiv \frac{1}{\nu} \int v_i v_j f d^3 \mathbf{v}. \quad (2.31)$$

Subtracting  $\overline{v_j}$  times the equation of continuity (2.28) and substituting

$$\sigma_{ij}^2 \equiv \overline{(v_i - \overline{v_i})(v_j - \overline{v_j})} = \overline{v_i v_j} - \overline{v_i} \overline{v_j} \quad (2.32)$$

gives the Jeans equations

$$\nu \frac{\partial \overline{v_j}}{\partial t} + \nu \overline{v_i} \frac{\partial \overline{v_j}}{\partial x_i} = -\nu \frac{\partial \Phi}{\partial x_j} - \frac{\partial (\nu \sigma_{ij}^2)}{\partial x_i}. \quad (2.33)$$

The Jeans equations (2.33) are the stellar-dynamical analogue to the ordinary Euler equation of hydrodynamics. Here  $\nu \sigma_{ij}^2$  is a stress tensor that describes an anisotropic pressure. Applying an analogous sequence of steps one can obtain the Jeans equations in cylindrical coordinates by taking moments of the CBE in cylindrical coordinates (see Binney & Tremaine, 1987);

$$\frac{\partial (\nu \overline{v_R})}{\partial t} + \frac{\partial (\nu \overline{v_R^2})}{\partial R} + \frac{\partial (\nu \overline{v_R v_z})}{\partial z} + \nu \left( \frac{\overline{v_R^2} - \overline{v_\phi^2}}{R} + \frac{\partial \phi}{\partial R} \right) = 0, \quad (2.34)$$

$$\frac{\partial (\nu \overline{v_\phi})}{\partial t} + \frac{\partial (\nu \overline{v_R v_\phi})}{\partial R} + \frac{\partial (\nu \overline{v_\phi v_z})}{\partial z} + \frac{2\nu}{R} \overline{v_\phi v_R} = 0, \quad (2.35)$$

and

$$\frac{\partial (\nu \overline{v_z})}{\partial t} + \frac{\partial (\nu \overline{v_R v_z})}{\partial R} + \frac{\partial (\nu \overline{v_z^2})}{\partial z} + \frac{\overline{v_R v_z}}{R} + \nu \frac{\partial \Phi}{\partial z} = 0. \quad (2.36)$$

In addition, we give the Jeans equations for a spherically symmetric system in steady state and for  $\overline{v_r} = \overline{v_\theta} = 0$ , calculated by integrating  $\overline{v_r}$  times the CBE in spherical coordinates, as

$$\frac{d(\nu \overline{v_r^2})}{dr} + \frac{\nu}{r} \left( 2\overline{v_r^2} - (\overline{v_\theta^2} + \overline{v_\phi^2}) \right) = -\nu \frac{d\Phi}{dr}. \quad (2.37)$$

### 2.3.2. A model for individual galaxies

The models for spiral galaxies consist of a disk component, a bulge, and an extended dark matter halo. They are constructed in dynamical equilibrium, adopting a method described by Hernquist (1993a). This method uses the fact that the lowest (second) order moments of the CBE are determined by the density distributions of the components. Since those are known from observations one can compute velocity moments and approximate the real distribution function in velocity space by known distribution functions (e.g., Gaussian) having these moments. This method is only an approximation but it can be assumed that the system initialized this way reaches an equilibrium state after a short evolution. Hereafter we describe the basic properties of the initial model.

We assume a **stellar disk** with a density which decreases exponentially with increasing cylindrical radius  $R = \sqrt{x^2 + y^2}$  (Freeman, 1970) and is described by isothermal sheets perpendicular to the disk plane (Bahcall & Soneira, 1980; Spitzer, 1942)

$$\rho_d(R, z) = \frac{M_d}{4\pi h^2 z_0} \exp\left(-\frac{R}{h}\right) \operatorname{sech}^2\left(\frac{z}{z_0}\right), \quad (2.38)$$

where  $M_d$  is the disk mass,  $h$  is the radial scale length, and  $z_0$  is a characteristic measure of the scale height perpendicular to the galactic plane. The scale height is assumed to be independent

of the galactocentric distance (van der Kruit & Searle, 1981, 1982). To construct a velocity ellipsoid of the disk with the density given in equation (2.38) one can use moments of the CBE. Observations of velocity dispersions in disk galaxies show that the radial velocity dispersion is proportional to the surface density (Freeman, 1970; Lewis & Freeman, 1989; Bottema, 1993; Binney & Merrifield, 1998) implying that

$$\overline{v_R^2} \propto \exp\left(-\frac{R}{h}\right). \quad (2.39)$$

For an isothermal sheet (here  $\overline{v_z^2}$  is independent of  $z$ ) the vertical velocity dispersion is related to the disk surface density,  $\Sigma(R)$ , by

$$\overline{v_z^2} \propto \pi G \Sigma(R) z_0. \quad (2.40)$$

Observations of edge-on disk galaxies suggest that  $z_0$  does not vary with radius and therefore  $\overline{v_z^2} \propto \Sigma(R)$  (van der Kruit & Searle, 1981, 1982; van der Kruit & Freeman, 1984; see Bottema (1993) for an overview).

A small note: For a stellar system in equilibrium with density  $\rho$ ,  $\nabla P = -\rho \nabla \Phi$  with the ‘‘pressure’’  $P = \rho \sigma_z$  (this is related to the functional form of the Jeans equation as an analogue to the Euler equation, see Binney & Tremaine, 1987). We then get

$$\frac{1}{\rho} \frac{\partial(\rho \overline{v_z^2})}{\partial z} = -\frac{\partial \Phi}{\partial z}. \quad (2.41)$$

Near the plane of a highly flattened system, Poisson’s equation can be approximated by

$$\frac{\partial^2 \Phi}{\partial z^2} = 4\pi G \rho. \quad (2.42)$$

Combining equations (2.41) and (2.42) gives

$$\frac{\partial}{\partial z} \left( \frac{1}{\rho} \frac{\partial \rho}{\partial z} \right) = -\frac{4\pi \rho G}{\sigma_z^2}, \quad (2.43)$$

assuming  $\sigma_z^2$  is independent of  $z$ . The solution to equation (2.43) for constant  $\sigma_z^2$  is

$$\rho = \rho_0 \operatorname{sech}^2 \left( \frac{z}{z_0} \right) \quad (2.44)$$

with

$$z_0 = \left( \frac{\sigma_z^2}{2\pi G \rho_0} \right)^{1/2}. \quad (2.45)$$

The asymptotic behaviour of  $\rho$  is described by

$$\operatorname{sech}^2 \left( \frac{z}{z_0} \right) \approx \begin{cases} 1 - \frac{z^2}{4z_0^2} & \text{for } z \ll z_0, \\ 4e^{-2z/z_0} & \text{for } z \gg z_0. \end{cases} \quad (2.46)$$

The velocity structure in the radial and vertical directions in the disk plane is determined by equations (2.39) and (2.40). To quantify the normalization constant in equation (2.39) it is

required that the radial dispersion at a critical radius  $R = R_{\text{crit}}$  is determined by the Toomre  $Q$  parameter (Toomre, 1964). A critical velocity dispersion for the local stability of a thin gravitating disk at a given radius  $R_{\text{crit}}$  is defined by

$$\sigma_R \Big|_{R_{\text{crit}}} > \frac{3.36G\Sigma}{\kappa}, \quad (2.47)$$

or defining the Toomre stability parameter  $Q$ :

$$Q \equiv \frac{\sigma_R \kappa}{3.36G\Sigma} > 1 \quad (2.48)$$

for the local stability of an axisymmetric disk. The epicyclic frequency  $\kappa$  is defined by

$$\kappa^2 = \frac{3}{R} \left( \frac{\partial\Phi}{\partial R} \right) + \left( \frac{\partial^2\Phi}{\partial R^2} \right). \quad (2.49)$$

Here  $\Phi$  is the total potential arising from all components of the galaxy model. For the models used in this lab we assume a critical radius of  $R_{\text{crit}} = 2.4h$ . This corresponds to the solar radius  $R_{\odot}$  if the model is scaled to the Milky Way.

To compute the azimuthal moments of the velocity field of the disk one needs the Jeans equation in cylindrical coordinates (2.34). For a star that lies close to the galactic equator, one can evaluate equation (2.34) at  $z = 0$ , and assume that  $(\partial\nu/\partial z) = 0$ , to find

$$\frac{R}{\Sigma} \frac{\partial(\Sigma \overline{v_R^2})}{\partial R} + R \frac{\partial(\overline{v_R v_z})}{\partial z} + \overline{v_R^2} - \overline{v_\phi^2} + R \frac{\partial\Phi}{\partial R} = 0 \quad (2.50)$$

if we substitute  $\nu$  with  $\Sigma$  in the limit of a thin disk with  $z = 0$ . Substituting the azimuthal velocity dispersion

$$\sigma_\phi^2 = \overline{(v_\phi - \bar{v}_\phi)^2} = \overline{v_\phi^2} - \bar{v}_\phi^2 \quad (2.51)$$

and  $R(\partial\Phi/\partial R) = v_c^2$ , where  $v_c$  is the circular speed, in equation (2.50) gives the relevant second moment of the CBE to compute moments of the azimuthal velocity dispersions according to

$$\sigma_\phi^2 - \overline{v_R^2} - \frac{R}{\Sigma} \frac{\partial(\Sigma \overline{v_R^2})}{\partial R} - R \frac{\partial(\overline{v_R v_z})}{\partial z} = v_c^2 - \bar{v}_\phi^2. \quad (2.52)$$

The azimuthal dispersion was chosen to be related to the radial dispersion via the epicyclic approximation

$$\sigma_\phi^2 = \overline{v_R^2} \frac{\kappa^2}{4\Omega^2} \quad (2.53)$$

where  $\Omega$  is the angular frequency and  $v_c$  is the circular velocity derived from the potential of all components by

$$\Omega^2 = \frac{1}{R} \frac{d\Phi_{\text{all}}}{dR}, \quad (2.54)$$

$$v_c^2 = R \frac{d\Phi_{\text{all}}}{dR}. \quad (2.55)$$

The equations (2.39), (2.40), and (2.53) fully specify the velocity ellipsoid in the disk plane. Assuming an exponential surface density profile for the disk and an exponential distribution for the radial velocity dispersion, equation (2.52) with equation (2.53) simplifies to

$$\overline{v_\phi^2} - v_c^2 = \overline{v_R^2} \left( 1 - \frac{\kappa^2}{4\Omega^2} - \frac{R}{h} + \frac{\partial(\ln \overline{v_R^2})}{\partial \ln R} + \frac{R}{\overline{v_R^2}} \frac{\partial(\overline{v_R v_z})}{\partial z} \right). \quad (2.56)$$

In addition, some softening has to be applied to  $\overline{v_R^2}$  at small radii (see Hernquist (1993a) for a detailed description). Velocities are then initialized by drawing  $v_z$  from a Gaussian with dispersion  $(\overline{v_z^2})^{1/2}$ , drawing  $v_R$  from a Gaussian distribution with dispersion  $(\overline{v_R^2})^{1/2}$ , computing  $\overline{v_\phi}$  from equation (2.56), and determining the random component by drawing from a Gaussian with dispersion  $(\sigma_\phi^2)^{1/2}$ .

The **dark matter halo** is assumed to follow a density profile that is characterized by isothermal spheres over some radial interval leading to a phenomenological potential–density pair of

$$\rho_h(r) = \frac{M_h}{2\pi^{3/2}} \frac{\alpha}{r_c} \frac{\exp(-r^2/r_c^2)}{r^2 + \gamma^2}, \quad (2.57)$$

$$\Phi_h(r) = -\frac{GM_h(r)}{r} + \frac{GM_h\alpha}{\sqrt{\pi}r_c} \text{Ei}\left(-\left(\frac{r}{r_c}\right)^2 - q^2\right), \quad (2.58)$$

where  $M_h$  is the total mass of the halo,  $r_c$  is a cutoff radius, and  $\gamma$  is a core radius. The normalization constant  $\alpha$  is defined by

$$\alpha = \left(1 - \sqrt{\pi}q \exp(q^2)(1 - \text{erf}(q))\right)^{-1}, \quad (2.59)$$

where  $q = \gamma/r_c$ . The halos are truncated exponentially at  $r_c$ . In general  $r_c$  is artificially small to reduce the computational task of integrating particles that are only loosely bound and do not affect the luminous component of the galaxy. For a non-rotating spherical system with a mass distribution like equation (2.57) we have

$$\overline{v_\theta^2} = \overline{v_\phi^2}. \quad (2.60)$$

The velocity dispersion is defined by the Jeans equation in spherical coordinates (see equation 2.37)

$$\frac{1}{\rho_h} \frac{d}{dr} (\rho_h \overline{v_r^2}) + 2\beta(r) \frac{\overline{v_r^2}}{r} = -\frac{d\Phi}{dr}, \quad (2.61)$$

where  $\beta(r)$  is defined as

$$\beta(r) \equiv 1 - \frac{\overline{v_\theta^2}}{\overline{v_r^2}} \quad (2.62)$$

and measures the degree of anisotropy. If the system is isotropic ( $\beta(r) = 0$ ,  $\overline{v_r^2} = \overline{v_\theta^2}$ ) one can integrate equation (2.61) to give

$$\overline{v_r^2} = \frac{1}{\rho_h(r)} \int_r^\infty \rho_h(r) \frac{d\Phi}{dr} dr \quad (2.63)$$

and

$$\overline{v_r^2} = \frac{1}{\rho_h(r)} \int_r^\infty \rho_h(r) GM(r) dr, \quad (2.64)$$

where  $\Phi$  includes the self-gravity of the halo and of all other components which contribute to the gravitational field and  $M(r)$  is the cumulative mass distribution. The absolute speeds of the particles are selected from

$$F(v, r) = 4\pi \left(\frac{1}{2\pi\sigma^2}\right)^{3/2} v^2 \exp\left(-\frac{v^2}{2\sigma^2}\right) \quad (2.65)$$

with

$$\int_0^{\infty} F(v, r) dv = 1. \quad (2.66)$$

The Cartesian velocities are then initialized from  $v$  assuming isotropy (see Hernquist, 1993a).

Observations of the **stellar bulge** of the Milky Way and external galaxies imply that they are spheroidal systems following an  $r^{1/4}$  surface density law. A simple density profile that reproduces the  $r^{1/4}$  law was proposed by Hernquist (1990) and is used for this galaxy model. The potential–density pair is

$$\rho_h(r) = \frac{M_b a}{2\pi r} \frac{1}{(r+a)^3} \quad (2.67)$$

and

$$\Phi(r) = -\frac{GM_b}{r+a} \quad (2.68)$$

with a cumulative mass distribution of

$$M(r) = M_b \frac{r^2}{(r+a)^2}. \quad (2.69)$$

$M_b$  is the total mass of the bulge and  $a$  is the scale length. The velocities are initialized in the same manner as for the halo.

For the simulations performed here we use the following **system of units** employed by Hernquist (1992, 1993b): gravitational constant  $G = 1$ , exponential scale length of the disk  $h = 1$  and mass of the larger disk  $M_d = 1$ . In these units the galaxy model has  $z_0 = 0.2$ ,  $M_h = 5.8$ ,  $\gamma = 1$ ,  $r_c = 10$ ,  $M_b = 1/3$ , and  $a = 0.1$ . Scaled to the physical properties of the Milky Way or M31 this translates to  $h = 3.5$  kpc and  $M_d = 5.6 \times 10^{10} M_{\odot}$ .

This model has been proven as a valuable collisionless equilibrium model for disk galaxies and has been tested with several applications (Hernquist, 1992, 1993b; Quinn et al., 1993; Heyl et al., 1994; Mihos et al., 1995; Heyl et al., 1996; Walker et al., 1996; Weil & Hernquist, 1996; Velazquez & White, 1999; Naab et al., 1999). Figure 2.1 shows some spherically averaged properties of the initial disk galaxy like the ratio of dark to luminous mass, the density, and the circular velocities of the individual components.

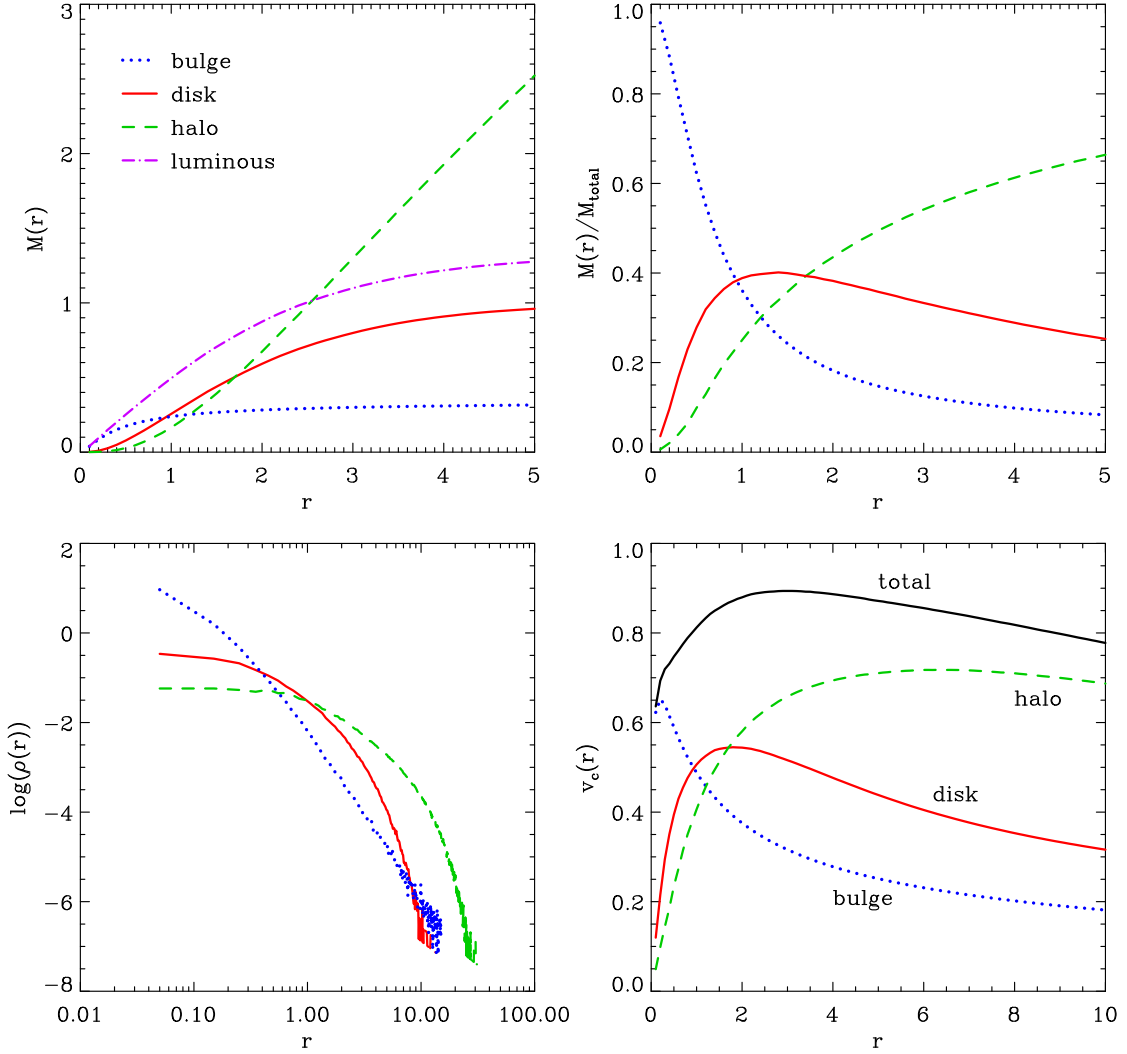


**Figure 2.1:** Spherically averaged properties of the initial disk galaxy vs. radius in units of disk scale lengths. *Upper left panel:* Cumulative mass of bulge (dotted), disk (solid), total luminous component (dash-dotted), and halo (dashed) vs. spherical radius. *Upper right panel:* Ratio of cumulative bulge, disk and halo mass and total cumulative mass vs. radius. *Lower left panel:* Density distribution for the different components. *Lower right panel:* Circular velocity of the model and separate contributions from disk, bulge, and halo vs. spherical radius. It has to be noted that the circular speed of the disk is underestimated by  $\approx 15\%$  since the mass is spherically binned and therefore assumed to be spherically distributed (see Binney & Tremaine, 1987).

# Chapter 3

## Exercise

The main goal of this exercise is to learn how to use a modern software for simulating and analysing  $N$ -body models of real galaxies. In a first step you will analyse an  $N$ -body model for a disk galaxy like our own Milky Way and use a simulation code to evolve the system in time. In a second step you will perform a merger between two disk galaxies and quantify the properties of the merger remnant.

As a first step, log in to the computer allocated for the  $N$ -body lab, either using the graphical interface or from a terminal by typing `ssh -4 -Y numprakt@mpusm06.usm.uni-muenchen.de` and, when asked, the password. Make a new folder for your group using the command `mkdir` and change into this folder using the command `cd`. Within this folder you can later create individual directories for every simulation you do and one directory in which you copy the macros to make the plots and where you can do the analysis of your simulations.

### 3.1. Fortran vs. Python lab

Depending on your choice, you can use the macros in `PRAKTIKUM/PROGRAMS/IDL`, which are written in IDL (**I**nter**I**ctive **D**ata **L**anguage) and follow closely the FORTRAN syntax of programming, or the macros in Python in `PRAKTIKUM/PROGRAMS/PYTHON`. The files have the same names but differ in the ending (`.pro` and `.py`, respectively).

Once you have copied the files into your own folder, you can edit the macros to make any changes to parameters (like location of files or other setting) or other parts as needed for the different exercises you will be doing. Then, you can run the macros in the following way:

- **IDL**: start IDL by typing `idl` (you should get an `IDL>` prompt) and then `.run macroname` (where you can omit the `.pro`). This either runs some program directly or it displays a list of available functions which you can then call by typing their names at the IDL prompt. To leave IDL and return to the shell, just type `exit`.
- **Python**: just type `python3.6 macroname.py` at the command line.

## 3.2. Getting used to the data

### 3.2.1. Setup

The  $N$ -body model for the disk galaxy has already been set up using the technique described in Section 2.3.2. You will find an ASCII version of the data set called `spiral.ascii` in the directory `PRAKTIKUM/DATA`. The 3-dimensional (`ndim=3`) system at time `t=0` contains in total `npart=20000` particles, with `6000` disk particles, `2000` bulge particles, and `12000` dark halo particles. The masses (`m`), positions (`x, y, z`) and velocities (`vx, vy, vz`) of all particles are stored in the following way:

```
npart,ndim,t
mass(1)
:
mass(npart)
x(1),y(1),z(1)
:
x(npart),y(npart),z(npart)
vx(1),vy(1),vz(1)
:
vx(npart),vy(npart),vz(npart)
```

### 3.2.2. Visualizing the initial conditions

As seen in the description above, the disk particles are always first, followed by the bulge and the halo particles. You can visualize this model using `show_ics`. This macro shows you the disk particles plotted in red and the bulge particles in blue.

**Q1. What is the morphological difference?**

**Q2. Plot the halo particles in addition.**

To do this, open the file `show_ics` with a text editor (e.g., `emacs`, `vi`, ...) and add an additional plot command for halo particles. The structure of the program is very simple. Where is the best place to add the additional command inside the macro? Make sure you plot the halo particles in a different colour! The `IDL` version plots the result on the screen (when executing the function `show_ics`) or creates a Postscript (`.ps`) file (when executing the function `print_ics`), while the `Python` version only produces a PDF (`.pdf`) file. You can view these files using the program `gv`.

## 3.3. Preparing vine\_3D

You will perform the simulations with the modern  $N$ -body tree-code **VINE**. The source code is in the directory `PRAKTIKUM/PROGRAMS/VINE_3D`. You can compile the code with the help of the `makefile` (have a look at the settings). To compile the code, you first have to supply a compiler, which you can do by typing `module load compiler`. Then, first remove all old compiled versions by typing `make clean` and then compile the code using simply `make`. When the code has been compiled you can copy the executable program `vine_3D` into your simulation directory.

### 3.4. Dynamical evolution of a single disk in isolation

First, create an own directory for every simulation you perform and copy into this directory the simulation code (`PRAKTIKUM/PROGRAMS/VINE_3D/vine_3D`) as well as the file with the initial conditions (e.g., `PRAKTIKUM/DATA/SPIRAL_000`), the parameter file (`PRAKTIKUM/DATA/insph`), and the job script (`PRAKTIKUM/DATA/runme.sh`). The binary versions of the initial conditions files are smaller than the corresponding ASCII files and better suited to store simulation data but are (historically) computer hardware specific. Therefore, do not forget to do `export F_UFMTENDIAN=big` on the command line before starting the simulations.

Before running the program, have a look at the input file `insph` and check the settings of all important parameters. This file is structured as follows:

```

'-----'
'Input/Output and Initialization'
'-----'
'Name of initialization and dump file..' 'base'      'SPIRAL_000'
'Use XDR library for I/O.....' 'iusexdr'    0
'Dump number for restart.....' 'idump'     0
'Make temporary dumps if itmpdmp=1....' 'itmpdmp'   1
'Time steps between SED etc outputs....' 'idmpfreq'  100
'Initial time step for all particles...' 'dtinit'    1d-2
'Maximum time in code units to end ....' 'tstop'     100d0
'Code time between dumps .....' 'dtdump'    1d0
'Debugging turn on if idbg>0.....' 'idbg'      1
'Print timing information if itme=1....' 'itme'      1
'-----'
...
'-----'
'Gravity settings'
'-----'
'Self gravity if igrav=1.....' 'igrav'     1
'Use GRAPE: igrave=1, else 0.....' 'igrave'    0
'Direct summation if 1, else tree.....' 'idirect'   0
'Timesteps between tree builds (globts)' 'maxbuild'  15
'Tree rebuild: if h_clmp>clfac*h_clmp0.' 'clhfrac'   5d0
'MAC: .angle(1).abserrWS(2).gadget(3)...' 'imac'      1
'MAC: opening criterion (angle or err)..' 'treeacc'   0.7d0
'Softening:0=varkern,1=fixkern,2=Plumr..' 'isoft'     2
'Plummer soft for isoft=1 .....' 'eps'       1d-1
'Max sep between clumps .....' 'sepmax'    10d0
'Minimum particles to send to GRAPE....' 'igrapelim' 50
'Max node mass for interaction list....' 'gmasslim'  1d100
'-----'
...

```

The important parameters for this exercise are `base`, being the name of the initial conditions file, `eps`, the gravitational softening length, and `dtinit`, the fixed time-step.

**Simulation 1:** Copy the initial conditions file `PRAKTIKUM/DATA/SPIRAL_000` into the directory you created and check that you have set the important parameters correctly in the `insph` file. Check that the force softening is set to `eps=1d-1`, the initial conditions file is the correct one (`base=SPIRAL_000`) and the time-step is set to `dtinit=1d-2`. Edit the job script `runme.sh` and assign a meaningful name to your simulation and ensure that the number of concurrently executing threads (`cpus-per-task`) is set to 4. Then start the program by typing `sbatch runme.sh`. Note the job ID (integer number) which is displayed. You can see if your job is running by typing `squeue` on the command line (you can find your job by the line containing the name you gave and the job ID you noted). The output is written into the file `slurm-ID.out` (where `ID` is the job ID), and you can follow the progress by typing `tail slurm-ID.out`.

The run will stop at time `t=100`. All units used are in **computational units** assuming that the gravitational constant `G=1`. Scaling the model disk to our Milky Way we can assume that the length unit `L=1` corresponds to 3.5 kpc and the mass unit `M=1` corresponds to  $5.6 \times 10^{10} M_{\odot}$ .

**Q3. Derive the physical time unit (in years) and the velocity unit (in km/s).** For this computation you will need the following constants:  $G = 6.672 \times 10^{-11} \text{ m}^3 \text{ kg}^{-1} \text{ s}^{-2}$ ,  $1 \text{ kpc} = 3.0856 \times 10^{19} \text{ m}$ ,  $1 M_{\odot} = 1.989 \times 10^{30} \text{ kg}$ .

When the run is finished it has created 100 dump files. To watch/analyse them, change into your directory with the plotting scripts and edit `plot_galaxy` where you have to set `basename` to `SPIRAL_`, `path` to the directory where you run the simulation, and `ndumps` to 100 (or the number of snapshots which are already there if the run is not yet finished). After running the script you will find a sequence of images in your directory showing the time evolution of the disk seen in face-on and edge-on projection. A simple way to watch the sequence of produced images is with the command `xv -wait 0 galaxy_*.png`.

For a more quantitative analysis use `plotvcirc` and edit it. You have to set `basename` to `SPIRAL_`, `path` to the directory where you run the simulation and `input.snap` to the snapshot that you want to analyse, so for the beginning set this to `0`. This program computes the circular velocity of the different components of the galaxy, their cumulative mass distribution and the projected surface density profiles of the disk and the bulge.

**Q4. Plot the same figure using physical units: km/s, solar masses, and solar masses per square parsec.** To do this, you can use the units you have computed before and edit the parameters `vscale`, `mscale`, and `sscale` in `plotvcirc`. In some of the analysis steps you might want to change the way quantities are plotted or to adapt the ranges for better view.

**Q5. How did the system properties change?** Now repeat the analysis for different time-steps up to `t=100` and discuss the results.

**Q6a. Parallelization efficiency:**

**Simulations 1a, 1b, 1c, 1d, and 1e:** Set up 5 variants of simulation 1 where you change the number of threads (`cpus-per-task`) to be 1, 2, 8, 16, and 32 in the job script `runme.sh`. Once the jobs are finished, the last line of the log file will tell you the wall-clock time it took.

**Create a plot!** Show the time needed as a function of the number of threads used. Can you interpret the plot? Is it what you would have expected?

**Q6b. Direct sum:**

**Simulation 1f:** Set up one more variant of simulation 1 by setting the opening angle `treeacc` in the parameter file to a very small value, making the criterion for using the tree very stringent and thereby effectively forcing the use of direct summation. This simulation will take quite long, so while it runs go ahead with the next steps. Later you can come back to this and add the wall-clock time for this simulation to the timing diagram of Q6a. Can you give an interpretation of the result?

**Q6c. Influence of the simulation parameters:**

**Simulations 2, 3, 4, and 5:** Set up 4 more variants of simulation 1. The gravitational softening length and the time-step are important parameters which guarantee the validity of the collisionless Boltzmann equation and therefore the stability of the system. To investigate the influence of them, perform 4 more simulations. In the first two, keep the original time step `dtinit=1d-2` and change the force softening `eps` in the file `insph` to `eps=1d-4` and `eps=1`, respectively. In the second 2 simulations keep the original force softening `eps=1d-1` but change the time-step to `dtinit=1d-1` and `dtinit=1d-3`. You can get an idea of the wall-clock time the individual simulations need by watching the time stamp associated with each of the dump files (type `ls -l` to see the file dates and times). When running the new simulations do not forget to make different directories for the different runs. Perform the same analysis and do not forget to save copies of the plots from the previous runs before overwriting them.

**What has changed?** Describe and interpret the differences in the simulations you can see.

### 3.5. A galaxy merger simulation

**Simulation 6:** Now run the simulation of the merger of two disk galaxies using a softening length of `eps=0.1` and the original time-step `dtinit=1d-2`. The initial conditions file `MERGER_000` can be found in `PRAKTIKUM/DATA` and has to be copied to your simulation directory and also needs to be set in the `insph` as `base=MERGER_000`.

As before, create the animation using `plot_merger` and create the profiles using `plotvcirc`. Remember all the changes you had to do to the programs before. As you will see, the disks rotate in the same direction. One disk is inclined by 30 degrees. During the merger the galaxies are perturbed and form extended tidal tails. The galaxies merge into one galaxy which appears to be spheroidal and not disk-like any more.

**Q7a. Discuss the changes.** Describe and interpret the changes in the cumulative mass and surface density profiles and changes in the velocity profile.

**Q7b. Timing.** Add the wall-clock time for the merger simulation, as well as for simulations 2, 3, 4, and 5 to the timing diagram of Q6a. Can you give an interpretation of the results?

### 3.6. Further interpretation and exploration

**Q8.** The surface density of the initial disk is given by

$$\Sigma = \Sigma_0 \times \exp(-r/r_d) \quad (3.1)$$

where  $r_d$  is the exponential scale length. What is the total mass of the disk? For disk systems the dynamical time can be defined as the rotation period at the half-mass radius of the disk. Compute the half-mass radius and the dynamical time for the initial disk component. What fraction of the dynamical time is the integration time step for the leapfrog integrator we have used?

**Q9.** For a homogeneous sphere with constant density  $\rho$  the mass inside of radius  $r$  is  $M(r) = \frac{4}{3}\pi r^3 \rho$ . What is the orbital period of a mass on a circular orbit? What is the equation of motion for a test particle released from rest at radius  $r$  in the gravitational field of a homogeneous body? How long does a particle need to reach  $r = 0$ ? This time scale is defined as the dynamical time for a (mostly spherical) system with a mean density  $\rho$ . Estimate the dynamical time (in physical units) of the total merger remnant at radii of 0.5, 1, 3, and 5 kpc. How does it compare to the (fixed) integration time-step?

**Q10.** Compute the half-mass radius of the bulge component of the disk model. What is the dynamical time of the bulge at this radius? Can we resolve bulge dynamics with the simulations performed here?

**Q11.** It is our goal to continually improve this exercise. Please let me know (either personally or by mail, [dolag@usm.lmu.de](mailto:dolag@usm.lmu.de)) if you have found errors, typos, or whether you have difficulties in understanding. I am also happy for any suggestions on how to improve it.



# Bibliography

- A. W. Appel: *SIAM J. Sci. Stat. Comp.* 6, 85 (1985)
- E. Athanassoula: *N*-body techniques and their impact on galactic stellar dynamics. In: F. Combes, E. Athanassoula (editors): *N*-body Problems and Gravitational Dynamics, page 116 (1993)
- J. N. Bahcall, R. M. Soneira: The universe at faint magnitudes. I. Models for the Galaxy and the predicted star counts. *The Astrophysical Journal Supplement Series* 44, 73 (1980)
- J. E. Barnes: Dynamics of galaxy interactions. In: R. C. Kennicutt Jr., F. Schweizer, J. E. Barnes, D. Friedli, L. Martinet, D. Pfenniger (editors): *Galaxies: Interactions and induced star formation*. Lecture notes, Saas Fee Advanced Course 26, page 276. Berlin: Springer (1998)
- J. E. Barnes: A hierarchical  $O(N \log N)$  force-calculation algorithm. *Nature* 324, 446 (1986)
- J. E. Barnes: Encounters of disk/halo galaxies. *The Astrophysical Journal* 331, 699 (1988)
- J. E. Barnes, L. Hernquist: Dynamics of interacting galaxies. *Annual Review of Astronomy and Astrophysics* 30, 705 (1992)
- J. E. Barnes, L. Hernquist: Transformations of galaxies. II. Gas dynamics in merging disk galaxies. *The Astrophysical Journal* 471, 115 (1996)
- K. Bekki: Unequal-mass galaxy mergers and the creation of cluster S0 galaxies. *The Astrophysical Journal Letters* 502, L133 (1998)
- K. Bekki, Y. Shioya: Formation of boxy and disky elliptical galaxies in early dissipative mergers. *The Astrophysical Journal Letters* 478, L17 (1997)
- R. Bender, R. L. Davies (editors): *New light on galaxy evolution*. IAU Symposium 171 (1996)
- R. Bender, P. Surma:  $Mg_2$  line-strength profiles of elliptical galaxies with kinematically decoupled cores. *Astronomy and Astrophysics* 258, 250 (1992)
- J. Binney, M. Merrifield: *Galactic Astronomy*. Princeton University Press (1998)
- J. Binney, S. Tremaine: *Galactic Dynamics*. Princeton University Press (1987)
- R. Bottema: The stellar kinematics of galactic disks. *Astronomy and Astrophysics* 275, 16 (1993)

- A. Burkert: Do elliptical galaxies have  $r^{1/4}$  brightness profiles? *Astronomy and Astrophysics* 278, 23 (1993)
- R. G. Carlberg: The phase space density in elliptical galaxies. *The Astrophysical Journal* 310, 593 (1986)
- R. L. Davies, E. M. Sadler, R. F. Peletier: Line-strength gradients in elliptical galaxies. *Monthly Notices of the Royal Astronomical Society* 262, 650 (1993)
- D. J. D. Earn, J. A. Sellwood: The optimal  $N$ -body method for stability studies of galaxies. *The Astrophysical Journal* 451, 533–541 (1995)
- S. M. Faber, S. Tremaine, E. A. Ajhar, Y. Byun, A. Dressler, K. Gebhardt, C. Grillmair, J. Kormendy, T. R. Lauer, D. Richstone: The centers of early-type galaxies with HST. IV. Central parameter relations. *Astronomical Journal* 114, 1771 (1997)
- R. T. Farouki, S. L. Shapiro: Simulations of merging disk galaxies. *The Astrophysical Journal* 259, 103 (1982)
- K. C. Freeman: On the disks of spiral and S0 galaxies. *The Astrophysical Journal* 160, 811 (1970)
- O. E. Gerhard:  $N$ -body simulations of disc-halo galaxies – Isolated systems, tidal interactions and merging. *Monthly Notices of the Royal Astronomical Society* 197, 179 (1981)
- L. Hernquist: Performance characteristics of tree codes. *The Astrophysical Journal Supplement Series* 64, 715 (1987)
- L. Hernquist: An analytical model for spherical galaxies and bulges. *The Astrophysical Journal* 356, 359 (1990)
- L. Hernquist: Structure of merger remnants. I. Bulgeless progenitors. *The Astrophysical Journal* 400, 460 (1992)
- L. Hernquist:  $N$ -body realizations of compound galaxies. *The Astrophysical Journal Supplement Series* 86, 389 (1993a)
- L. Hernquist: Structure of merger remnants. II. Progenitors with rotating bulges. *The Astrophysical Journal* 409, 548 (1993b)
- L. Hernquist, P. Hut, J. Makino: Discreteness noise versus force errors in  $N$ -body simulations. *The Astrophysical Journal Letters* 402, L85 (1993a)
- L. Hernquist, P. J. Quinn: Formation of shell galaxies. I. Spherical potentials. *The Astrophysical Journal* 331, 682 (1988)
- L. Hernquist, D. N. Spergel: Formation of shells in major mergers. *The Astrophysical Journal Letters* 399, L117 (1992)
- L. Hernquist, D. N. Spergel, J. S. Heyl: Structure of merger remnants. III: Phase-space constraints. *The Astrophysical Journal* 416, 415 (1993b)

- J. S. Heyl, L. Hernquist, D. N. Spergel: Structure of merger remnants. IV: Isophotal shapes. *The Astrophysical Journal* 427, 165 (1994)
- J. S. Heyl, L. Hernquist, D. N. Spergel: Structure of merger remnants. V: Kinematics. *The Astrophysical Journal* 463, 69 (1996)
- J. E. Hibbard, W. D. Vacca: The apparent morphology of peculiar galaxies at intermediate to high redshifts. *Astronomical Journal* 114, 1741 (1997)
- J. E. Hibbard, J. H. van Gorkom: HI, HII, and R-band observations of a galactic merger sequence. *Astronomical Journal* 111, 655 (1996)
- J. E. Hibbard, M. S. Yun: Luminosity profiles of merger remnants. *The Astrophysical Journal Letters* 522, L93 (1999)
- R. W. Hockney, J. W. Eastwood: *Computer simulations using particles*. McGrawHill Inc. (1981)
- J. G. Jernigan: Direct  $N$ -body simulations with a recursive center of mass reduction and regularization. In: J. Goodman, P. Hut (editors): *Dynamics of star clusters*. IAU Symposium 113, page 275 (1985)
- J. G. Jernigan, D. H. Porter: A tree code with logarithmic reduction of force terms, hierarchical regularization of all variables, and explicit accuracy controls. *The Astrophysical Journal Supplement Series* 71, 871 (1989)
- J. Kormendy, R. Bender: A proposed revision of the Hubble sequence for elliptical galaxies. *The Astrophysical Journal Letters* 464, L119 (1996)
- J. R. Lewis, K. C. Freeman: Kinematics and chemical properties of the old disk of the Galaxy. *Astronomical Journal* 97, 139 (1989)
- J. C. Mihos, L. Hernquist: Gasdynamics and starbursts in major mergers. *The Astrophysical Journal* 464, 641 (1996)
- J. C. Mihos, I. R. Walker, L. Hernquist, C. Mendes De Oliveira, M. Bolte: A merger origin for X structures in S0 galaxies. *The Astrophysical Journal Letters* 447, L87–L90 (1995)
- I. F. Mirabel, L. Vigroux, V. Charmandaris, M. Sauvage, P. Gallais, D. Tran, C. Cesarsky, S. C. Madden, P. Duc: The dark side of star formation in the Antennae galaxies. *Astronomy and Astrophysics* 333, L1 (1998)
- T. Naab, A. Burkert, L. Hernquist: On the formation of boxy and disky elliptical galaxies. *The Astrophysical Journal Letters* 523, L133 (1999)
- J. Negroponte, S. D. M. White: Simulations of mergers between disc-halo galaxies. *Monthly Notices of the Royal Astronomical Society* 205, 1009 (1983)
- J. P. Ostriker, S. D. Tremaine: Another evolutionary correction to the luminosity of giant galaxies. *The Astrophysical Journal Letters* 202, L113 (1975)
- P. J. Quinn, L. Hernquist, D. P. Fullagar: Heating of galactic disks by mergers. *The Astrophysical Journal* 403, 74 (1993)

- D. Rigopoulou, H. W. W. Spoon, R. Genzel, D. Lutz, A. F. M. Moorwood, Q. D. Tran: A large mid-infrared spectroscopic and near-infrared imaging survey of Ultraluminous Infrared Galaxies: Their nature and evolution. *Astronomical Journal* 118, 2625 (1999)
- H. Rix, C. M. Carollo, K. Freeman: Large stellar disks in small elliptical galaxies. *The Astrophysical Journal Letters* 513, L25 (1999)
- G. B. Rybicki: Relaxation times in strictly disk systems. *Astrophysics and Space Science* 14, 15–19 (1971)
- D. B. Sanders, I. F. Mirabel: Luminous Infrared Galaxies. *Annual Review of Astronomy and Astrophysics* 34, 749 (1996)
- L. J. Spitzer: The dynamics of the interstellar medium. III. Galactic distribution. *The Astrophysical Journal* 95, 329 (1942)
- V. Springel: Modelling star formation and feedback in simulations of interacting galaxies. *Monthly Notices of the Royal Astronomical Society* 312, 859 (2000)
- A. Toomre: On the gravitational stability of a disk of stars. *The Astrophysical Journal* 139, 1217 (1964)
- A. Toomre: Mergers and Some Consequences. In: B. Tinsley, R. Larson (editors): *The evolution of galaxies and stellar populations* (New Haven: Yale Univ. Press), page 401 (1977)
- A. Toomre, J. Toomre: Galactic bridges and tails. *The Astrophysical Journal* 178, 623 (1972)
- P. C. van der Kruit, K. C. Freeman: The vertical velocity dispersion of the stars in the disks of two spiral galaxies. *The Astrophysical Journal* 278, 81 (1984)
- P. C. van der Kruit, L. Searle: Surface photometry of edge-on spiral galaxies. I – A model for the three-dimensional distribution of light in galactic disks. II – The distribution of light and colour in the disk and spheroid of NGC 891. *Astronomy and Astrophysics* 95, 105 (1981)
- P. C. van der Kruit, L. Searle: Surface photometry of edge-on spiral galaxies. III – Properties of the three-dimensional distribution of light and mass in disks of spiral galaxies. *Astronomy and Astrophysics* 110, 61 (1982)
- H. Velazquez, S. D. M. White: Sinking satellites and the heating of galaxy discs. *Monthly Notices of the Royal Astronomical Society* 304, 254 (1999)
- I. R. Walker, J. C. Mihos, L. Hernquist: Quantifying the fragility of galactic disks in minor mergers. *The Astrophysical Journal* 460, 121 (1996)
- M. L. Weil, L. Hernquist: Global properties of multiple merger remnants. *The Astrophysical Journal* 460, 101 (1996)
- R. L. White: Noise and relaxation in simulations of disk galaxies. *The Astrophysical Journal* 330, 26–37 (1988)
- S. D. M. White: Simulations of merging galaxies. *Monthly Notices of the Royal Astronomical Society* 184, 185 (1978)

S. D. M. White: Further simulations of merging galaxies. *Monthly Notices of the Royal Astronomical Society* 189, 831 (1979)

C. D. Wilson, W. E. Harris, R. Longden, N. Z. Scoville: Two Populations of Young Massive Star Clusters in Arp 220. *The Astrophysical Journal* 641, 763 (2006)

R. F. G. Wyse: Phase-space density constraints on the formation of bulges from discs. *Monthly Notices of the Royal Astronomical Society* 293, 429 (1998)